PAPER

A novel bioassay based gold nanoribbon biosensor to aid the preclinical evaluation of anticancer properties†

Seetharamaiah Nalini,[ad] Seetharamaiah Nandini,[ad] M. B. Madhusudana Reddy,[b] Gurukar Shivappa Suresh,*[a] Jose Savio Melo,*[c] Shivayogeeswar E. Neelagund,*[d] Hunasepalya Nagaiah NaveenKumar[d] and Sangaraju Shanmugam[e]

In this work, we report a microbial biosensor fabricated for the preclinical assay of anticancer compounds. Gold nanoribbons were used as a transducer for mounting the microbe. For the synthesis of these unique Au nanostructures, quercetin stabilized gold nanoparticles (Q-AuNPs) were synthesized as a first step using onion peel. Later, dityrosine peptide was used as a sacrificial template for the synthesis of the gold nanoribbons (AuNRs). The structural morphology of the as-synthesized Au nanomaterial was examined using UV spectroscopy, XRD, SEM and TEM. The AuNRs were found to be <10 nm in diameter, which provided a good biocompatible environment and effective protection for the immobilization of *Agrobacterium tumefaciens* (*At*), a causative agent of crown gall disease. *At* is reported to cause tumors in plants through a tumorigenic mechanism similar to that of humans. Inhibition of *At* indicates that the inhibitory compound being screened exhibits anticancer activity. *Clitoria ternatea* (*Ct*) is traditionally used to cure many diseases and is known to possess anticancer activity. Therefore, we have used a *Ct* flower extract in the preclinical study of its anticancer activity against *At* by fabricating a simple electrochemical sensor. We have employed electrochemical techniques such as CV and EIS for the characterization of the developed microbial biosensor. Moreover, the as-synthesized AuNRs behave as an ideal transducer and platform, thus improving the electrode surface area and providing good biocompatibility for the immobilization of *At*. In contrast to other immobilization techniques and biosensors that often require elaborate procedures, cross-linking agents and rigorous chemical reactions, *At* was directly adsorbed onto the electrode under optimum conditions without any mediators. The results show that the developed biosensor is useful in the pre-clinical analysis of anticancer properties. Indeed the study examines the use of electrochemistry, demonstrating the rapid response and high sensitivity of the proposed sensor in contrast to bioassay procedures. In conclusion, the experimental results indicate that the developed biosensor accentuates the excellent properties of the synthesized AuNRs, which promises to be a novel avenue in designing biosensors.

[a]Department of Chemistry and Research Centre, N.M.K.R.V. College for Women, Jayanagar, Bangalore 560 011, India. E-mail: sureshssmrv@yahoo.co.in; Fax: +91-80-22453665; Tel: +91-80-26654920

[b]School of Chemistry, Reva University, Kattigenahalli, Yelahanka, Bangalore 560064, India

[c]Nuclear Agriculture and Biotechnology Division, Bhabha Atomic Research Centre, Mumbai 400 085, India. E-mail: jsmelo@barc.gov.in

[d]Department of PG Studies and Research in Biochemistry, Jnana Sahyadri, Kuvempu University, Shankaraghatta, Shivamogga-577 451, Karnataka, India. E-mail: neelgund@gmail.com

[e]Department of Energy Systems and Engineering, Daegu Gyeongbuk Institute of Science and Technology, Daegu 711-873, Republic of Korea

† Electronic supplementary information (ESI) available. See DOI: 10.1039/c6ra07501k

1. Introduction

Cancer is a terrible and highly fatal illness characterized by anomalous cell growth caused by mutations in normal cells.[1] It is known to be a major reason for mortality throughout the world. The invention of new drugs that can combat cancer is of great interest to many researchers. In the current era, many plants have been documented to treat cancer; for instance vinca alkaloids are used against leukemia, *Podophyllum* is used for small lung and testicular cancer, *Taxus* spp. is antagonistic to skin cancers and *Taxus brevifolia* is inimical to ovarian and breast cancer.[2] *Clitoria ternatea* (*Ct*) is one such plant that has been documented to alleviate an extensive variety of ailments. It belongs to the *Fabaceae* family with common names such as 'Butterfly pea', 'Aprajita', 'Shankupushpi' and 'Girikarnika'. It is shown to have antidepressant, anticonvulsant, antioxidant,

anesthetic and sedative, hypoglycemic, anthelmintic, anxiolytic, antidote, hypoglycemic and anticancer properties.[3-6] Several glycosides such as malvidin-3-β-glycoside, delphinidin-3-β-glycoside, anthocyanins, ternatins (C1–C5 and O3) and pre-ternatins (A3 and A4) have been reported to exist in the plant. The flowers of *Ct* have also been reported to contain many therapeutic bioactive compounds.[7,8] This gives a brief outline of how plants have made a contribution in drug discovery research.

Thousands of new compounds for cancer treatment are being invented by researchers and scientists across the globe, very few of which compounds are considered for clinical analysis owing to factors such as cost and ethical considerations. Thus a pre-screening method is essential. The intention behind this process is to recognize and select the compounds which act against cancer in order to promote them to the next level in clinical research. Nevertheless, the pre-screening method should be rapid, uncomplicated and affordable with a favorable prognosis of pharmacodynamic activity.[9,10]

In recent years electrochemical techniques have gained precedence over the conventional methods of analysis owing to the fact that they possess a greater sensitivity, with low cost and a relatively short analysis time when compared with other analytical techniques. Efforts have been made in the research area of analytical electrochemistry in the quest for the development of electrochemical biosensors that are capable of meeting the essential requirements. Nanomaterials such as nanowires, nanotubes and nanocrystals have been extensively used as the transducing element in the development of biosensors due to their promising and unique properties.[11] Gold nanoparticles (AuNPs), nanoribbons, nanobelts, quantum dots, zinc oxide, silver, platinum, palladium, carbon nanotubes, graphene *etc.* are some of the examples of nanomaterials that are known to increase the performance of biosensors in terms of the selectivity, sensitivity and long term stability.[12-19] In particular, the synthesis of 1D Au metal nanostructures such as nanowires, nanotubes, nanobelts and nanoribbons is given exceptional consideration in this field as they are known to improve optical, thermal and electronic properties.[20,21] Apart from this, they are also used widely in the fields of fuel cells, batteries and super capacitors. Some challenges are faced by the scientific community that hinder the development of these nanostructures, including the need for simple, facile, low cost and high yielding preparative methods.[22] 1D nanostructures are of great importance compared to bulk metal nanoparticles mainly due to their simple preparative procedures and better catalytic activity.[23] The synthesis of the nanostructures can be carried out as reviewed[22,24] using methods such as template assisted growth, electrochemical beam irradiation, electrochemical deposition *etc.* Palladium nanowires synthesized by electron beam irradiation are reported to have good electrocatalytic activity and stability for ethanol oxidation.[25] In addition, an alloy of Pt–Co alloy nanowires showed excellent electrocatalytic activity towards methanol oxidation.[26] Likewise, Pd–Ag nanotubes were reported to exhibit superior electrocatalytic activity towards formic acid oxidation.[27] MnO_2 nanotube and nanowire arrays were fabricated using galvanostatic electrodeposition on a porous alumina template.[28] At this point, it is important to state that our group is also actively involved in the synthesis of Au nanostructures. We have reported gold nanoparticle nanotubes (AuNPNTs) employing an alumina membrane as a template[29] and Au nanotubes synthesized using β-diphenyl-alanine (β-FF) as a sacrificial template.[30] These nanostructures were applied in the development of biosensors for the determination of hydrogen peroxide and cholesterol respectively.

Apart from electrochemical analysis, bioassays are a set of procedures in which a compound (drug, pesticide, fungicide *etc.*) is tested for its activity against biological entities (an animal, bacterial cells, human cancer cells *etc.*). The capability of the tested compounds to suppress the biological entities is considered to correlate to their activity as therapeutic agents. Bioassays benefit standardization when analyzing the active bioactive compound in plant extracts. The isolation of a bioactive compound in a plant extract from heterogeneous compounds by physical and analytical methods can be subtle because the chemical complexity and the relative amount present may vary from each process of the isolation technique. In many instances, the therapeutic activity exhibited by the plant's bioactive compound is not due to a single constituent but a combination of many constituents. Therefore, analytical techniques take a back seat.[31] To date, one available technique is the potato disc tumor assay which is considered as the simplest bioassay approach to determine the anticancer activity of crude plant extracts. Volumes of manuscripts have been published giving evidence of the benefits of utilizing this method.[2,32-36] The principle that this assay is based on is the antimitotic inhibition of *Agrobacterium tumefaciens* (*At*) induced tumors in potato. *Agrobacterium tumefaciens* is a Gram negative bacterium which causes crown gall tumors in more than 60 families of dicotyledonous plants, some monocots and some gymnosperms.[37] The tumor induction involves a unidirectional mechanism in which a small segment of T-DNA present in a 190 kb T_i (tumor inducing) plasmid is transferred into the plant genome. The incorporated T-DNA gene encodes enzymes, namely tryptophan mono-oxygenase, indoleacteamide hydrolase and isopentenyl transferase. The first two enzymes aid in the conversion of tryptophan to indoleacetic acid (auxin) and the latter converts AMP to cytokinin isopenetenyl adenosine (cytokine). The overproduction of these plant hormones (auxin and cytokinin) results in uncontrolled growth of tissue and gall formation on the crown, roots and in some other parts of the plants.[38-40] The significance of crown gall disease is that it is similar to human cancer, *i.e.*, the cellular mechanism with reference to chemical reactions such as the type IV secretion system is the same in these members of the two kingdoms.[41-44] It has already been reported that compounds which vanquish *At* may show activity in the 3PS leukemic mouse assay and 9KB or 9PS cytotoxicity assays and therefore can be considered as an anticancer drug in humans.[2,45] Therefore *Agrobacterium tumefaciens* can be used in anticancer studies.[46,47]

As a solution to the acknowledged problem, in this manuscript we have attempted to develop a novel biosensor based on Au nanoribbons (AuNRs). Initially, quercetin stabilized Au nanoparticles (Q-AuNPs) were prepared. This is because colloidal gold solutions are not stable for a long duration in the

native state. Therefore, we isolated quercetin from onion peels and used it as a stabilizing agent. The uniqueness of this work is the synthesis of gold nanoribbons using dityrosine peptides as a structure directing agent for the synthesis of AuNRs and the electrochemical application of the as-synthesized AuNRs for the bioassay. The dityrosine peptides afford controlled growth of the nanoribbons along the longitudinal axis of the template, preventing aggregation of the nanoparticles. This is the first report, to the best of our knowledge, on the application of these peptides as a sacrificial template for AuNRs. The AuNRs behave as an ideal transducer and platform, thus improving the electrode surface area and providing good biocompatibility for the immobilization of *At*. In contrast to other immobilization techniques and biosensors that often require elaborate procedures, cross-linking agents and rigorous chemical reactions, the *At* was directly adsorbed onto the electrode under optimum conditions without any mediators. Furthermore, a biosensor fabricated using the AuNRs as an immobilizing matrix for *At* to study the preclinical anticancer screening has not been reported so far. This electrochemical approach is simple and offers high sensitivity and excellent selectivity. We have also demonstrated that the sensor operates at a low working potential, thereby eliminating the possible interfering electroactive substances. The practical applicability of the sensors towards H_2O_2 detection was also verified.

2. Materials and methods

2.1. Materials

Gold(III) chloride hydrate ($HAuCl_4$), *N,N'*-dicycloxicarbodiimide (DCC) and *N*-methylmorpholine (NMM) were procured from Sigma Aldrich. Isopropyl alcohol, chloroform sodium bicarbonate ($NaHCO_3$), sodium sulfate (Na_2SO_4), ethanol and methanol were purchased from Rankem, India. 1,1,1,3,3,3-Hexafluro-2-propanol (HFIP) was purchased from Spectrochem, India. Luria Bertani Agar Miller was purchased from Himedia for the isolation and growth of *Agrobacterium tumefaciens* (*At*). A PK-3 electrode polishing kit containing 1 μm aqueous polishing diamond and 0.05 μm polishing alumina was obtained from BAS Inc. Tokyo, Japan. Phosphate buffer saline was prepared from a stock solution of 0.1 M KH_2PO_4, 0.1 M K_2HPO_4 and 0.1 M KCl. The pH was adjusted using 0.5 M HCl and 0.5 M NaOH. 30% H_2O_2 was obtained from Merck.

2.2. Electrochemical measurements

All electrochemical experiments were carried out with Versa-STAT 3 (Princeton Applied Research, USA). A field emission scanning electron microscope (FE-SEM), Hitachi S-4800II model, with an accelerating voltage of 5 kV was utilized to observe the surface morphologies of the electrodes and the elemental analysis of the electrodes was carried out by energy dispersive X-ray analysis (EDAX). All experiments were done in a conventional three electrode electrochemical cell with bare Gr and a modified electrode (Gr/AuNR/*At*) as the working electrode, a saturated calomel electrode as the reference electrode and platinum wire as the auxiliary electrode.

3. Experimental

3.1. Extraction of plant material

Flowers of *Ct* were obtained from Idappadi taluk, Salem district, Tamilnadu. The taxonomical characterization of the plant was confirmed with the help of a professional botanist. The flowers were cleaned gently, air dried and powdered coarsely. The powdered flower was soxhlet extracted with ethanol for 2 hours, followed by vacuum filtration, and the powder was discarded. The excess solvent was removed and the extract was concentrated by distillation. Finally, the ethanol extract was accurately weighed and dissolved in water to a concentration of 0.2 mg mL^{-1} for our electrochemical studies.

3.2. Extraction of quercetin from *Allium cepa* (onion) for the synthesis of quercetin stabilized AuNPs

Fresh onions were collected from a local market. The collected sample was cleaned with tap water and subsequently washed with pure water. The bulbs were separated and the tunics were sliced and dried in the shade for 2–3 days. As a first approach, about 750 g of the dried sample was pulverized into a coarse powder and subjected to soxhlation with petroleum ether. The so-obtained extract was filtered and concentrated to dryness overnight at room temperature. The extract was then partitioned into two equal fractions. These partitioned fractions were extracted separately, each with 85% methanol and 90% ethanol for 12 h for isolation of quercetin. The methanolic extract and ethanolic extract obtained in this way were mixed in equal volumes and then concentrated to dryness. Screening of the products was done by TLC and the desired compound was purified by column chromatography. The isolated quercetin was characterized and confirmed by UV, IR and mass spectroscopy (results not shown). Finally, its melting point and structure were determined.

3.3. Synthesis of AuNPs

The procedure for the synthesis of quercetin stabilized AuNPs (Q-AuNPs) comprises the following steps. A solution of $HAuCl_4$ was first prepared by dissolving 0.393 g of metal precursor in 1.5 mL of isopropanol under an argon atmosphere using a glove box. To this, a few mL of pure water was added at room temperature and the solution was irradiated by ultrasonication for 3 minutes to obtain a homogeneous suspension. At this point, 20 mL of a 0.1 M aqueous solution of freshly extracted quercetin was added swiftly while irradiating the solution at an intensity of 100 W cm^{-2}. The reaction mixture changed to a red wine colored solution within 15 min, indicating the formation of AuNPs. However, in order to ensure the complete reduction of Au(III) ions to AuNPs, ultrasonication was continued for further time. The product was obtained by repeated washings and centrifugation. The as-synthesized Q-AuNPs were investigated by UV-Vis spectroscopy, XRD, SEM and EDAX.

3.4. Synthesis of AuNRs

In the present work, we have employed a novel route for the synthesis of one dimensional metal nanostructures in which

dityrosine peptide serves as a structure directing agent for the synthesis of AuNRs. For the fabrication of the dityrosine building block, the dipeptide was initially synthesized following a reported procedure.[48] Briefly, 0.04 g carboxyl protected tyrosine peptide (H_2N-Tyr-OMe) was added to 250 mL round bottom flask and suspended in $CHCl_3$ (25 mL). This solution was cooled to 0 °C and a solution of 2.23 mL NMM was added and stirred for 30 min. Subsequently, to the stirred solution 0.04 g of Boc-protected tyrosine (Boc-Tyr-OH) dissolved in $CHCl_3$ was added. After a few minutes of stirring, the coupling of the dipeptide was accomplished using 2.1 g DCC. The ice bath was removed and the reaction mixture was stirred at room temperature for 24 h. The solvent was then removed by filtration and the residue was given multiple washings with $CHCl_3$. The resulting residue was resuspended in the filtrate and washed with 5% $NaHCO_3$ and saturated NaCl. The organic fraction was dried (Na_2SO_4), filtered and concentrated under reduced pressure. Finally, the resulting product was re-crystallized and analyzed by mass spectroscopy.

The experimental procedure was then extended for the self-assembly of the dityrosine peptide exploiting the Reches and Gazit procedure.[49] The purified dityrosine peptide was dissolved in HFIP at a concentration of 100 mg mL^{-1} and then diluted with water at a concentration of 2 mg mL^{-1}, leading to the formation of the self-assembled peptide structures. Subsequently, we focused on the synthesis of AuNRs using the self-assembled dipeptide. To grow one dimensional Au nanostructures, the Q-AuNPs obtained above were mixed with the self-assembled dityrosine peptide solution at a concentration ratio of 4 : 1 (gold to peptide solution).[50] This mixture was allowed to stand in the dark at a temperature of 4 °C for at least an overnight time period to allow optimum binding of the Q-AuNPs on the peptide substrate. The formation of the one dimensional Au nanostructure was easily determined visually with the formation of a red precipitate at the bottom of the vial. The obtained precipitate was collected by centrifugation, washed and dispersed in water by ultrasonic irradiation. The peptide–Q-AuNP solution was found to be stable against ultrasonication as revealed by the subsequent SEM analysis. This was followed by proteolytic cleavage[50] for the facile release of the desired AuNRs. This method relies on the use of proteinase K by incubating it with the peptide–Q-AuNP ensemble solution at a concentration of 100 µg mL^{-1} for 1 h at 37 °C in 50 mM Tris–HCl (pH 7.5) containing 10 mM $CaCl_2$. The peptide cleavage procedure degrades the dityrosine peptide and ejects the well defined metal coated AuNRs AuNRs. Notably, in practice the detachable template reported in this manuscript has impressive thermal stability, mechanical stability and cost effectiveness. The peptide solution remained stable for more than one year, providing a strong indication that it can be considered as an alternative substrate for the traditional template directed synthesis with good results.

3.5. Preparation of microbial suspension

Agrobacterium tumefaciens was grown in Luria Bertani Agar Miller, with an incubation period of 28–30 °C for 18–24 h. After 24 h, a solid white mass deposit was observed. This was centrifuged; the solid deposit was collected, suspended in

distilled water and centrifuged again. The cell mass was suspended in 0.5 mL of 0.9% NaCl and successive dilutions were done to determine the density of the biomass spectrophotometrically at 560 nm. The cell suspension used for the development of the biosensor was freshly prepared before the experiment and the viable cells was in their growth curve corresponding to the log-phase of bacterial cells (OD_{560} = 0.6).

3.6. Development of electrochemical biosensor

An electrode was prepared by drilling a Teflon bar to a 6 mm diameter and a graphite (Gr) cylinder was introduced into it. Electrical contact was made with a copper wire through the center of the Teflon bar. Prior to modification, the Gr electrode was polished to get a mirror shine surface by means of a PK-3 electrode polishing kit. It was then ultrasonicated for several minutes and rinsed with pure water to remove adhered impurities. To this cleaned surface 5 µL of AuNRs were drop-casted and this was kept overnight. Later, 5 µL of *At* cell suspension was added and allowed to stand for about 20 min at room temperature. This modified microbial biosensor is termed Gr/AuNR/*At* henceforward in this manuscript. The schematic representation of the preparation of the electrode is shown in Fig. 1.

4. Results and discussion

4.1. Structural characterization of Q-AuNPs using UV-Vis spectroscopy, XRD and SEM

All metal nanoparticles display a characteristic intense color depending on the surface plasmon resonance band (SPR). The position of this SPR relates to the size, shape and extinction coefficient of the NPs. Therefore the optical properties of the Q-AuNPs were investigated using UV-Visible spectroscopy. Fig. 2A shows the typical extinction spectra of the as-synthesized NPs recorded in the spectral range 400–700 nm. The Q-AuNPs exhibit a single and sharp SPR peak centered at 532 nm implying the formation of isotropic AuNPs with uniform size.

Furthermore to investigate the phase transition and crystallographic structure, we examined the XRD pattern of the Q-AuNPs. The representative X-ray powder diffraction spectrum of the sample synthesized by ultrasonic irradiation is illustrated in Fig. 2B. The peaks of the diffraction pattern were observed at 2θ = 38.3°, 44.5° and 64.5° corresponding to the [111], [200] and [220] reflection peaks of the face centered cubic structure of Au. This result correlates to the reported literature[51] indicating successful formation of the Q-AuNPs. The average particle size of the Q-AuNPs calculated from the obtained XRD data using the Scherrer equation is found to be 10.5 nm.

The structural morphology of the Q-AuNPs was further elucidated by SEM measurements. It is evident from the SEM image (Fig. 2C) that the Q-AuNPs exhibit good spherical features. The particle size of the individual particles estimated using ImageJ software is about 10 nm or smaller and the corresponding size distribution histogram (see ESI S1†) is given in Fig. 2D. The average particle diameter estimated from these histogram graphs is found to be reasonably consistent with our
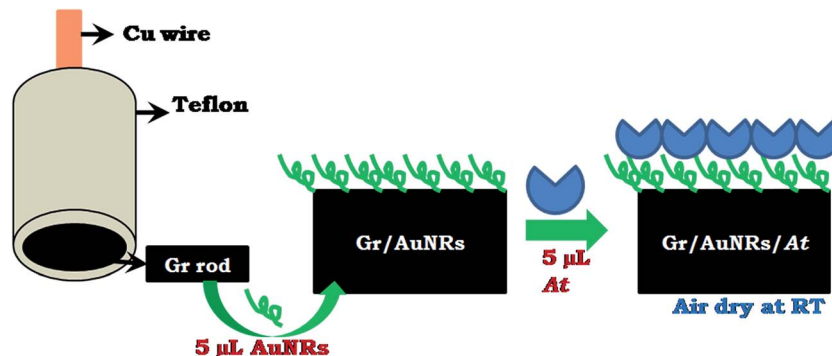
Fig. 1 Schematic illustration for fabricating the Gr/AuNR/*At* electrode.

XRD data and it's seen that all the nanoparticles are uniform in distribution.

4.2. Physical characterization of the self-assembled dipeptide, Q-AuNP–peptide ensemble and AuNRs using SEM, TEM and EDAX

We have also investigated the structural morphology of self-assembled dipeptide, Q-AuNP–dipeptide ensemble and AuNRs by SEM. The structural details of the self-assembled dipeptide (Fig. 3A) reveals truncated cable-like self-assembled micro-structures. Evidently, Q-AuNPs seem to completely cover the surface of the peptide networks as shown in Fig. 3B for the Q-AuNP–dipeptide ensemble. It appears that the microstructure is comprised of multiple Q-AuNPs with a narrow size distribution. Following proteolytic cleavage, the morphological characteristics of the peptide microstructure–Au ensemble template showed an individual ribbon-like morphology with 100 nm diameter (Fig. 3C). It is found that the nanoribbon is uniform in diameter throughout its longitudinal axis. Notably, this is the
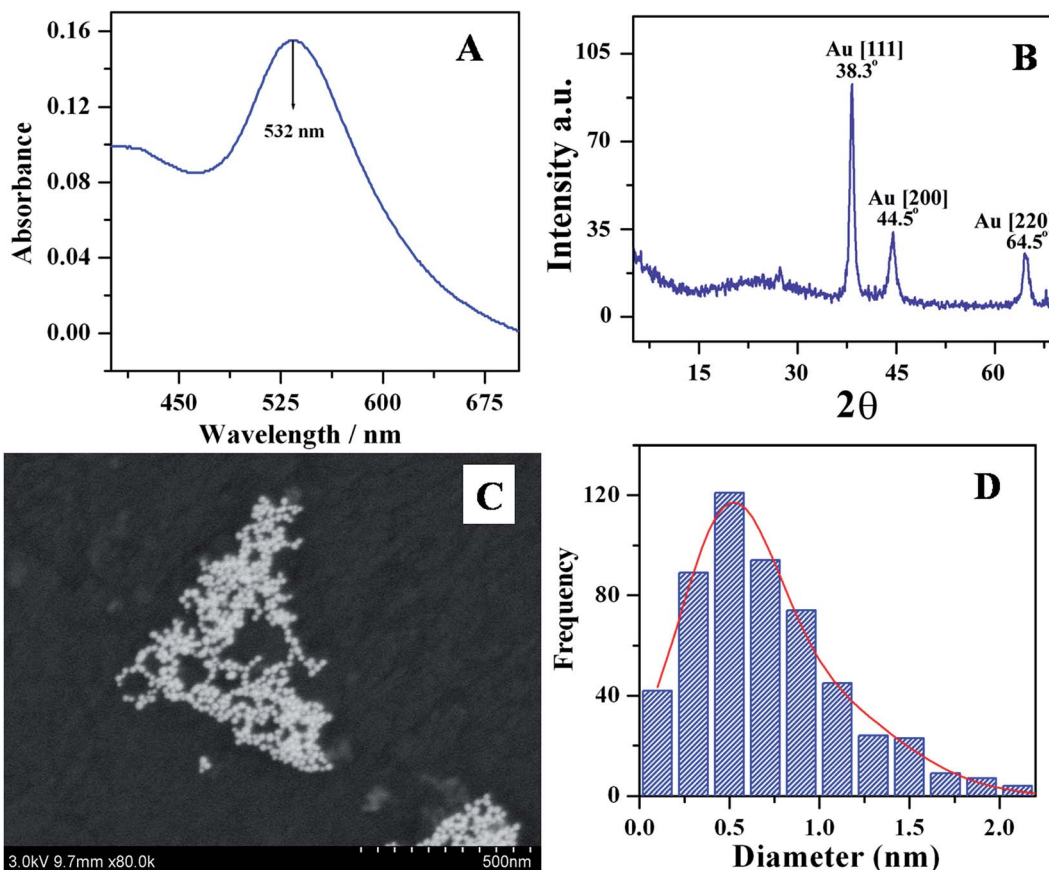

Fig. 2 (A) UV-Vis spectra of Q-AuNPs in the spectral range from 400–700 nm. (B) X-ray diffraction pattern of Q-AuNPs. (C) Scanning electron micrograph of Q-AuNPs; (D) corresponding histogram of size distribution of Q-AuNPs.
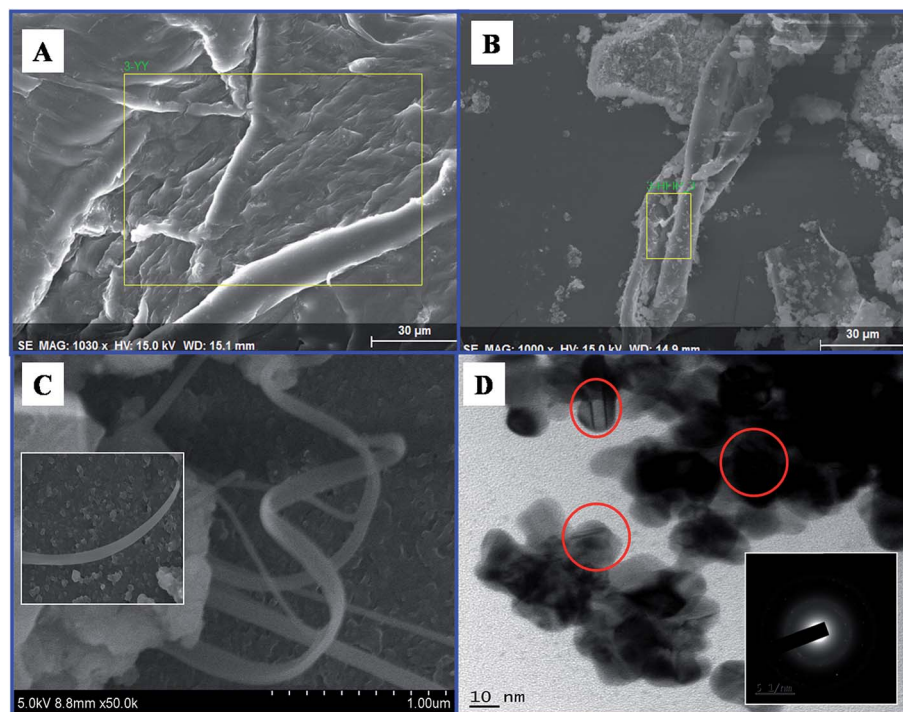
Fig. 3 SEM images of (A) self-assembled peptide, (B) Q-AuNP–peptide ensemble and (C) AuNRs. (D) A TEM image of AuNRs; the circled parts show individual nanoribbon entities. Inset shows a corresponding electron diffraction pattern.

first report on the synthesis of AuNRs that has been achieved using dityrosine as a detachable template. These SEM micrographs suggest that the dityrosine peptides' typical ribbon-like micro-architecture is expected to be responsible for the formation of ordered Au nanoribbons. Furthermore, transmission electron microscopy (TEM) was performed to investigate the diameter of the as-synthesized nanoribbons (Fig. 3D). The figure clearly demonstrates the presence of a number of nanostructures with an average diameter of <10 nm which depends on the diameter of the structure directing dityrosine template. Interestingly, the structural features of most of the particles revealed a well-defined one dimensional nanostructure. The inset shows the corresponding electron diffraction pattern of the AuNRs. Consequently, EDAX was employed to provide qualitative information on the elements and the contents of the as-prepared nanostructures. The typical EDAX of these samples is given in ESI.†

4.3. Electrochemical impedance spectroscopic studies for the modified electrodes

Cyclic Voltammetry (CV) and electrochemical impedance spectroscopy (EIS) were used for examining each stepwise modification of the electrodes – bare Gr, AuNRs and Gr/AuNR/*At* in 0.1 M PBS containing 1 mM $K_3[Fe(CN)_6]/K_4[Fe(CN)_6]$. As seen in Fig. 4A the bare Gr electrode gave a CV spectrum with the least peak current whereas, when AuNRs were drop cast onto the electrode surface, the CV spectrum exhibited a significant enhancement in current. This was obviously due to the presence of AuNRs, with their excellent electrocatalytic properties leading

to the enhancement of current. In contrast, as expected, Gr/AuNR/*At* restricts the electron conduction of $K_3[Fe(CN)_6]/K_4[Fe(CN)_6]$. This may be due to the poor electron conductivity property of the bacterium. This gives evidence of the successful modification of the electrodes.

EIS is an effective method to study the surface modification characteristics of electrodes. The results obtained for the impedance measurement can be depicted in two ways: (a) a Nyquist plot and (b) a Bode plot. In the Nyquist plot (Fig. 4B), the data is acquired as a real part *vs.* an imaginary part and the semi-circular part corresponds to the electron transfer resistance while the straight line is converse to the diffusion limited electrochemical process. In contrast, the Bode plot provides information on the impedance, frequency and phase angle. It is expressed as logarithmic values of the impedance modulus *vs.* the frequency '*f*'.[52] As shown in Fig. 4C the Bode magnitude plot consists of three phases. The frequency range from 1 kHz to 100 kHz is a linear plot which corresponds to the conduction of ions between the electrodes from the electrolyte while the frequency range from 1 Hz to 100 Hz represents the double layer capacitance and the range from 100 mHz to 1 Hz symbolizes the charge transfer resistance and faradic impedance. As a consequence, if the electrode material is resistant to ferricyanide ions, it displays a horizontal line in the Bode magnitude plot and a Bode phase plot close to 0°. In the case that it has capacitance ability, it is represented by a straight line with a slope of −1 in the log *Z*–log *f* representation and a phase angle of 90°. In contrast, the diffusion controlled phenomenon of an electrode material would give a straight line with a slope of −1/2 and a phase angle of 45°.[53] An interpretation of the modification
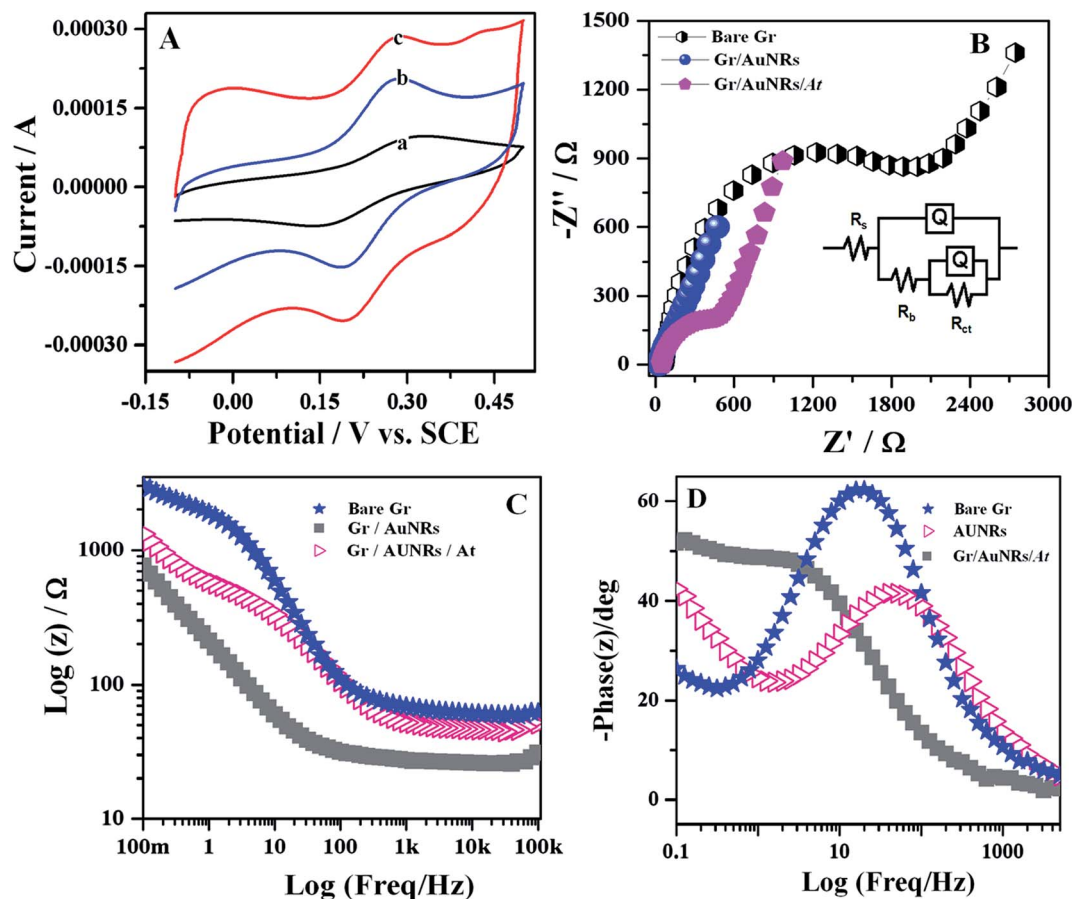
Fig. 4 (A) Cyclic voltammograms, (B) Nyquist plots, (C) Bode magnitude plot and (D) Bode phase plot for bare Gr, Gr/AuNRs and Gr/AuNR/*At* in a solution of 5 mM $K_3[Fe(CN)_6]/K_4[Fe(CN)_6]$.

of each electrode was determined by evaluating the shape of the Bode plot. A general decline in the impedance and phase angle indicated modification. As evident from Fig. 4C, the impedance of the AuNRs was less compared to Gr/AuNR/*At* and bare Gr. This may be due to the presence of AuNRs which exhibit good electrocatalytic activity with a least impedance plot whereas the presence of *At* in the Gr/AuNR/*At* electrode led to an increase in impedance due to its non-conductive nature in $K_3[Fe(CN)_6]/K_4[Fe(CN)_6]$ solution. Further evaluation of the phase angle (Fig. 4D) also supported the evidence presented by the impedance plot with the order bare Gr ($\sim$62°) > Gr/AuNRs/*At* ($\sim$48°) > AuNRs ($\sim$41°), *i.e.*, the lesser the phase angle the higher the electron conductivity.

The behavior of the electrode is represented by fitting the impedance data (Table 1) to an equivalent circuit (Fig. 4B inset). The CV spectra, Nyquist plots and Bode plots are in good agreement with the experimental and theoretical results. The equivalent circuit obtained consists of R_s, the solution resistance which is connected parallel to the double layer capacitance and R_f, the film resistance. The double layer capacitance is represented by a constant phase element Q_1 and Q_2. Q_1 is also parallel to the sub-circuit R_f. In the second compartment Q_2 is parallel to R_{ct}, the charge transfer resistance. The R_s values of all the electrodes were found to be approximately the same, which

indicates that the solution resistance and the diffusion of the $K_3[Fe(CN)_6]/K_4[Fe(CN)_6]$ ions are not exaggerated by biochemical reactions occurring at the electrode interface. The electron transfer resistance, R_{ct}, of Gr was estimated to be 5.345 kΩ. In contrast the Gr/AuNRs showed a straight line in the Nyquist plot with an R_{ct} value of 0.001 kΩ. Such a slight decrease in R_{ct} might be ascribed to the excellent conductivity of the AuNRs whereas the highest R_{ct} value of 202.3 kΩ was exhibited by Gr/AuNR/*At*. This increase of R_{ct} indicates the adhesion of bacteria to the AuNRs. The R_{ct} reflects an increase in Q_1 values. The Q_1 values indicate a decrease in space between the electrode material and the active center. The increase in Q_1 leads to an enhancement of the film thickness, leading to a decreased capacitance with an increased dielectric constant and film capacitance, Q_2. This will result in a decrease in film resistance, R_f.[54] From these results it can be concluded that the electrode has been successfully modified.

4.4. Cyclic voltammetry studies of different modified electrodes

CV was used to study the electroanalytical properties of the microbial biosensor. Fig. 5 shows the CV spectra obtained after each modification of the Gr electrode in 0.1 M PBS at a scan rate of 0.05 V s^{-1} and a potential range from 1.2 to -0.6. The CV of

**Table 1**   EIS data of bare Gr, Gr/AuNRs and Gr/AuNR/*At*

Electrode	R_s (Ω)	R_f (kΩ)	R_{ct} (kΩ)	$Q_1 \times 10^{-6}$ (Ω^{-1} cm^{-2})	n	$Q_2 \times 10^{-3}$ (Ω^{-1} cm^{-2})	n
Bare Gr	28.64	2.23	5.345	0.4	0.8	0.9	0.8
Gr/AuNRs	24.65	0.488	0.001	0.8	0.8	1.2	0.8
Gr/AuNR/*At*	26.64	6.877	202.3	1.1	0.7	1	0.6

bare Gr (Fig. 5a) did not show any cathodic or anodic peak whereas the Gr/AuNR electrode Fig. 5b displayed a well defined anodic peak at 0.8 V and a cathodic peak at 0.5 V with an increment in the current response. These peaks correspond to the occurrence of Au nanostructures drop casted onto the bare Gr surface. This indeed indicates the tight adhesion of the Au particles. Further, the CV of the Gr/*At* electrode exhibited a redox peak (Fig. 5c) at around 0.2 V. Obviously, this can be attributed to the existence of electroactive metabolites in the bacterium which act as mediators in the electron transfer, revealing the redox peaks. In contrast, when 5 μL of *At* was introduced along with the AuNRs, the CV spectrum Fig. 5d displayed the combined peaks of Au and *At* as seen in Gr/AuNR and Gr/*At*. These superfluous peaks are termed a, a′ and b, b′ for Au peaks and *At* peaks respectively, and this can be attributed to the successful immobilization of *At* on AuNR/Gr. The anodic and cathodic peaks observed were relatively large compared to Gr/*At* and Gr/AuNR. The AuNRs played a pivotal role in the modification of the electrode. They not only increased the current response, but also increased the surface area of the electrode, providing more vacant space for occupancy of the bacterium, thereby resulting in the fast electrochemical phenomenon. This confirms the successful development of the Gr/AuNR/*At* electrode.

4.5. Electro-catalysis of *At* immobilized on Gr/AuNRs

The electro-catalytic activity of the immobilized *At* was determined by studying the effect of an increasing concentration of H_2O_2. This is because the bacterium is well known to possess

oxidase and catalase activity.[34] Fig. 6A shows the behavior of the microbial biosensor in the presence and absence of H_2O_2. Upon addition of the substrate, the reduction peak of Au (a′) and *At* (b′) increased with a concomitant decrease in the anodic peak, demonstrating the efficiency of *At* and Au for the consumption of H_2O_2 and thus the liberation of oxygen at the electrode surface. This can also be attributed to the action of the component enzymes (catalase and oxidase) embedded in the bacterium, essentially to shield the microbe by dissolving the noxious peroxides and super oxides.

$$2H_2O_2 \underset{At}{\rightarrow} H_2O + O_2 \tag{1}$$
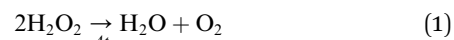
From this it can be concluded that the bacterium is stable on the electrode surface, on which the AuNRs provide a good environment for the attachment of the bacterium. Fig. 6B depicts the calibration curve as a function of H_2O_2 concentration, obtained using CV. It can be observed that as the concentration H_2O_2 increases from 0 to 8 mM, the peak current increases linearly. The linear regression equations are as follows:

$$I_{p\ AuNRs} = -1.246 \times 10^{-4} + 1.84 \times 10^{-5} C_{Ct}\ (\mu M);\ R = -0.999 \tag{2}$$

$$I_{p\ At} = -7.770 \times 10^{-5} + -1.827 \times 10^{-5} C_{Ct}\ (\mu M);\ R = -0.999 \tag{3}$$

Fig. 6C shows the CV spectrum obtained for the Gr/AuNR/*At* electrode in 0.1 M nitrogen saturated PBS at different scan rates. With an increasing scan rate from 10 mV s^{-1} to 300 mV s^{-1}, the redox peak current increases. This is can be attributed to the AuNRs, which proves that the decrease in size tends to increase with the surface to volume ratio leading to the rigid adsorption of the bacterium. As shown in the Fig. 6D both I_{pa} and I_{pc} exhibit a linear dependence on the scan rates, indicating that the electron transfer process for Gr/AuNR/*At* is a surface controlled process.

The linear regression equations for anodic and cathodic peak currents are as follows:

$$I_{pa\ AuNRs} = 2.867 \times 10^{-4} + 3.578 \times 10^{-7} v\ (V\ s^{-1});\ R = 0.979 \tag{4}$$

$$I_{pc\ AuNRs} = -2.449 \times 10^{-5} + -9.763 \times 10^{-6} v\ (V\ s^{-1});\ R = -0.991 \tag{5}$$

$$I_{pa\ At} = 8.167 \times 10^{-5} + 4.288 \times 10^{-7} v\ (V\ s^{-1});\ R = 0.994 \tag{6}$$

$$I_{pc\ At} = -4.675 \times 10^{-5} + -5.588 \times 10^{-7} v\ (V\ s^{-1});\ R = 0.988 \tag{7}$$
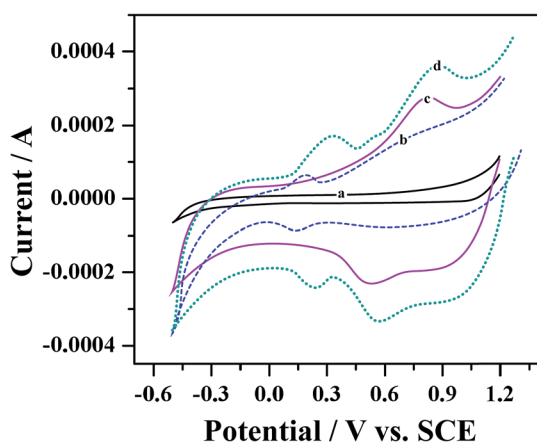

Fig. 5   Cyclic voltammograms of the electrode modified with different components: (a) bare Gr, (b) Gr/*At*, (c) Gr/AuNR and (d) Gr/AuNR/*At*.
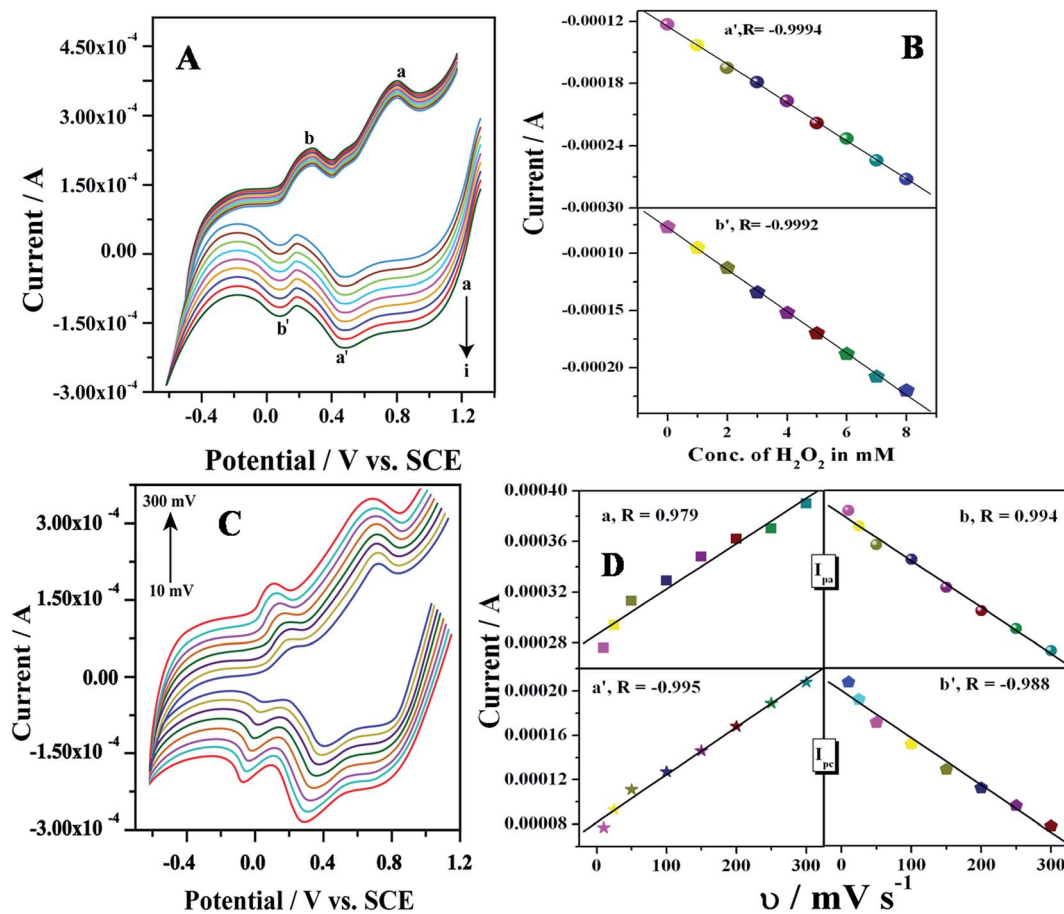
Fig. 6 (A) Cyclic voltammograms of Gr/AuNR/*At* in the presence of various concentrations of H_2O_2 in 0.1 M PBS (pH 7) at a scan rate of 50 mV s^{-1}, in which a and b correspond to the AuNR and *At* oxidation peaks and a' and b' correspond to the AuNR and *At* reduction peaks. (B) The calibration plot obtained from Gr/AuNR/*At* in the presence of various concentrations of H_2O_2. (C) Cyclic voltammograms of Gr/AuNR/*At* at various scan rates: 10, 25, 50, 100, 150, 200, 250 and 300 mV s^{-1} in 0.1 M PBS. (D) The redox peak currents of AuNRs and *At* on scan rates.

4.6. The effect of an increasing concentration of the *Ct* extract on the Gr/AuNR/*At* microbial sensor

CV was used to characterize the effect of injection of the *Ct* extract into an electrochemical cell containing the Gr/AuNR/*At* microbial sensor. As shown in Fig. 7A, the addition of the *Ct* extract decreases the peak current of the microbial sensor at around 0.2 V in comparison with the absence of extract. As the concentration of the added *Ct* extracts increased from 100 μL of 0.2 mg mL^{-1} of *Ct*, the peak current decreased concomitantly whereas the prominent current peaks displayed by the AuNRs remained unchanged. This may be due to the phytochemical constituents present in the *Clitoria ternatea* ethanolic extract which suppress the activity of *Agrobacterium tumefaciens* leading to the drop-off in peak current, while having no effect on the AuNRs. The *At* peak diminished after addition of 500 μL of the extract. As described in the introduction, *At* is the causative agent of crown gall disease which is characterized by uncontrolled growth of stems and root tissues. These tumors are histologically similar to human tumors. Therefore, the inhibition of crown gall disease by active compounds or drugs shows a relationship to their antitumor activity in humans. From this

it can be concluded that the Gr/AuNR/*At* microbial sensor can be used in bioassays of anticancer drugs.

4.7. Chronoamperometric study of the anticancer activity of *Clitoria ternatea* ethanolic extract on the Gr/AuNR/*At* microbial sensor and determination of the selectivity of the developed biosensor

The amperometric determination of the effect of the *Ct* extract on *At* was studied under stirring conditions in 0.1 M PBS at 0.2 V. After stabilization of the baseline current, the *Ct* extract was injected at intervals of 30 s in increasing concentrations and the response was recorded. It was noted that the current response decreased. This decrease indicates the viability of the bacterium to survive. Fig. 7B clearly shows the fast response and high sensitivity of the Gr/AuNR/*At* microbial sensor towards the *Ct* extract. The response time in our proposed biosensor is less than 3 s in contrast to a conventional bioassay which requires a minimum of 12 days to a maximum 15–20 days. The developed biosensor was compared with existing methods used to pre-screen the anticancer activity of therapeutic compounds and the results are shown in Table 2.[2,32–35,46] The dose response
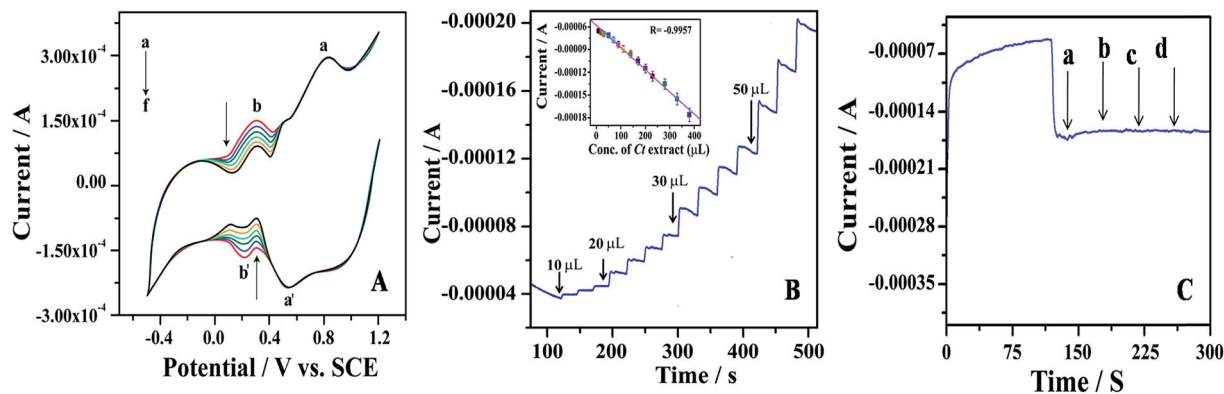
Fig. 7 (A) Cyclic voltammograms of Gr/AuNR/*At* exposed to increasing concentrations of 10 μL of *Ct* extract in 0.1 M PBS. (B) Chronoamperometry of the developed microbial sensor in a stirred 0.1 M PBS solution after addition of increasing concentrations of *Ct* extract at the applied potential of −0.2 V. Inset: the linear calibration plot of the inhibition current *vs. Ct* extract with error bars at the standard deviation. (C) The amperometric response of the modified bioelectrode to successive additions of (a) 2 mM cholesterol and interferences, (b) 1 mM AA, (c) 0.5 mM UA and (d) 1 mM ACT in 0.1 PBS at pH 7.

Table 2 Comparison of the results of the fabricated electrochemical biosensor with reported bioassay procedures

Time required for analysis	Reference
Potato disc assay	
12 days	2
3 weeks	32
12 days	33
2 weeks	34
12 days	35
12 days	46
Electrochemical biosensor	
<3 s	This work

curve was plotted as the concentration of the *Ct* extract injected *vs.* the current response exhibited by *At* (figure not shown). The inhibition concentration (IC$_{50}$) value was found to be 13.61 μg mL^{-1}. These results show that the ethanolic extract of *Ct* is toxic to *At*.

To investigate the selectivity of the developed biosensor for H$_2$O$_2$ over interfering substances, sequential additions of 2 mM H$_2$O$_2$, 1 mM ascorbic acid (AA), 0.5 mM uric acid (UA) and 1 mM acetaminophen (ACT) were measured into a stirring solution of 0.1 M PBS (pH 7). The results are shown in Fig. 7C. The addition of H$_2$O$_2$ caused a significant signal, while the addition of UA, AA and ACT did not cause any electrochemical or current change. This indicates high selectivity for H$_2$O$_2$, but no interference for UA, AA and ACT.

5. Conclusions

Preclinical screening is essential before subjecting active compounds for further investigation to develop drugs. Electrochemical assays could be used as an aid in the screening of potential anticancer compounds. The advantages of the electrochemical study over conventional bioassays, such as cost,

reduced time and ease of preparation of the biosensor, are obvious from the current work. The electrochemical study could be a substitute for animal models or it could lessen the pain of the experimental animals. The results of this study show a definite correlation for the activity of the *Ct* extract towards *At*. The calculated IC$_{50}$ value was 13.61 μg mL^{-1}. From the study we conclude that the microbial biosensor could be the first criterion for further investigation in pharmacodynamics.

References

1 D. W. Hoskin and A. Ramamoorthy, *Biochim. Biophys. Acta*, 2008, **1778**, 357.
2 P. S. Coker, J. Radecke, C. Guy and N. D. Camper, *Phytomedicine*, 2003, **10**, 133.
3 A. P. Patil and V. R. Patil, *Int. J. Pharm. Pharm. Sci.*, 2011, **3**, 330.
4 K. Madhu, *Asian J. Pharm. Clin. Res.*, 2013, **6**, 38.
5 R. Kavitha and V. Premalakshmi, *Int. J. Pharma Bio Sci.*, 2013, **4**, 236.
6 R. A. Jain, S. H. Shukla and A. K. Saluja, *Int. J. Pharm. Sci. Res.*, 2010, **12**, 88.

7   G. D. Neda, M. S. Rabeta and M. T. Ong, *Int. Food Res. J.*, 2013, **20**, 1229.

8   V. Ramaswamy, N. Varghese and A. Simon, *Int. J. Drug Discovery*, 2011, **3**, 74.

9   A. M. Burger and H. H. Fiebig, *Handbook of Anticancer Pharmacokinetics and Pharmacodynamics*, ed. W. D. Figg and H. L. McLeod, Humana Press Inc., Totowa, NJ, 1st edn, 2004, ch. 2, pp. 29–43.

10 A. M. Burger and H. H. Fiebig, *Handbook of Anticancer Pharmacokinetics and Pharmacodynamics*, ed. M. A.Rudek, C. H. Chau, W. D. Figg and H. L. McLeod, Springer, New York, 2nd edn, 2014, ch. 2, pp. 23–38.

11 J. M. Pingarron, P. Yanez-Sedeno and A. Gonzalez-Cortes, *Electrochim. Acta*, 2008, **53**, 5848.

12 X. Zhang, Q. Guo and D. Cui, *Sensors*, 2009, **9**, 1033.

13 B. Garipcan, M. Caglayan and G. Demirel, *New Perspectives in Biosensors Technology and Applications*, ed P. A. Serra, InTech, Croatia, 2010, ch. 9, pp. 197–214.

14 Y. Shao, J. Wang, H. Wu, J. Liu, I. A. Aksay and Y. Lin, *Electroanalysis*, 2010, **22**, 1027.

15 M. Pumera, S. Sanchez, I. Ichinose and J. Tang, *Sens. Actuators, B*, 2007, **123**, 1195.

16 Z. Qiang, R. Yuan, Y. Q. Chai, N. Wang, Y. Zhuo, Y. Zhang and X. F. Li, *Electrochim. Acta*, 2006, **51**, 3763.

17 Y. F. Li, Z. M. Liu, Y. L. Liu, Y. H. Yang, G. L. Shen and R. Q. Yu, *Anal. Biochem.*, 2006, **349**, 33.

18 M. G. Li, Y. J. Shang, Y. C. Gao, G. F. Wang and B. Fang, *Anal. Biochem.*, 2005, **341**, 52.

19 S. Sagadevan and M. Periasamy, *Rev. Adv. Mater. Sci.*, 2014, **36**, 62.

20 H. Lan, Z. Yu, G. Zhirui and G. Ning, *Chin. Sci. Bull.*, 2009, **54**, 1626.

21 K. Tomizaki, S. Wakizaka, Y. Yamaguchi, A. Kobayashi and T. Imai, *Langmuir*, 2014, **30**, 846.

22 J. N. Tiwari, R. N. Tiwari and K. S. Kim, *Prog. Mater. Sci.*, 2012, **57**, 724.

23 Y. Zhong, C. L. Xu, L. B. Kong and H. L. Li, *Appl. Surf. Sci.*, 2008, **255**, 3388.

24 Y. Xia, P. Yang, Y. Sun, Y. Wu, B. Mayers, B. Gates, Y. Yin, F. Kim and H. Yan, *Adv. Mater.*, 2003, **15**, 353.

25 F. Ksar, G. Surendran, L. Ramos, B. Keita, L. Nadjo, E. Prouzet, P. Beaunier, A. Hagege, F. Audonnet and H. Remita, *Chem. Mater.*, 2009, **21**, 1612.

26 J. N. Tiwari, R. N. Tiwari, Y. M. Chang and K. L. Lin, *ChemSusChem*, 2010, **3**, 460.

27 Y. Lu and W. Chen, *J. Phys. Chem. C*, 2010, **114**, 21190.

28 H. Xia, J. Feng, H. Wang, M. O. Lai and L. Lu, *J. Power Sources*, 2010, **195**, 4410.

29 S. Nandini, S. Nalini, J. Sanetuntikul, S. Shanmugam, P. Niranjana, J. S. Melo and G. S. Suresh, *Analyst*, 2014, **139**, 5800.

30 S. Nandini, S. Nalini, M. B. Madhusudana Reddy, G. S. Suresh, J. S. Melo, P. Niranjana, J. Sanetuntikul and S. Shanmugam, *Bioelectrochemistry*, 2016, **110**, 79.

31 J. L. Mclaughin and L. L. Rogers, *Drug Inf. J.*, 1998, **32**, 513.

32 M. S. Islam, M. M. Rahman and M. J. Alam Nurunnahar, *Plant Env. Dev.*, 2008, **2**, 87.

33 F. O. Bryant, H. G. Cutler and S. R. Parker, *J. Nat. Prod.*, 1994, **57**, 640.

34 M. Soriful Islam, M. Munsina Akter, M. Atikur Rahman and M. Mostafizur Rahman, *Curr. Res. Bacteriol.*, 2010, **3**, 27.

35 N. R. Ferrigni, J. E. Putnam, B. Anderson, L. B. Jacobsen, D. E. Nichols, D. S. Moore, J. L. Mclaughin, R. G. Poisell and C. R. Smith, *J. Nat. Prod.*, 1982, **45**, 679.

36 A. A. Amara, M. H. EL-Masry and H. H. Bogdady, *Pak. J. Pharm. Sci.*, 2008, **21**, 159.

37 C. W. Lee, M. Efetova, J. C. Engelmann, R. Kramell, C. Wasternack, J. Ludwig-Muller, R. Hedrich and R. Deeken, *Plant Cell*, 2009, **21**, 2948.

38 I. Onyesom, *Educ. Res. Rev.*, 2006, **1**, 12.

39 A. Rhouma, A. Boubaker, X. Nesme and Y. Deasaux, *Tunis. J. Plant Prot.*, 2006, **1**, 73.

40 A. Miranda, G. Janssen, L. Hodges, E. G. Peralta and W. Ream, *J. Bacteriol.*, 1992, **174**, 2288.

41 A. C. Braun, *Prog. Exp. Tumor Res.*, 1972, **15**, 165.

42 E. M. Lai and C. I. Kado, *Trends Microbiol.*, 2000, **8**, 361.

43 A. C. Braun and T. Stonier, *Protoplasmatologia*, 1958, **10**, 1.

44 E. F. Smith, *Science*, 1912, **35**, 161.

45 A. A. Amara, *Aust. J. Crop Sci.*, 2013, **1**, 1.

46 A. Hussain, M. Zia and B. Mirza, *Turk. J. Biol.*, 2007, **31**, 19.

47 A. M. M. Ibrahim, M. H. Mostafa, M. H. El-Masry and M. M. A. El-Naggar, *Egypt. J. Aquat. Res.*, 2005, **31**, 146.

48 R. Dahiya, *Acta Pol. Pharm.*, 2007, **64**, 509.

49 M. Reches and E. Gazit, *Science*, 2003, **300**, 625.

50 K. Lu, V. P. Conticello and D. G. Lynn, *Mater. Res. Soc. Symp. Proc.*, 2004, **826**, V1.6.

51 Y. Chen, X. Gu, C. G. Nie, Z. Y. Jiang, Z. X. Xie and C. J. Lin, *Chem. Commun.*, 2005, **33**, 4181.

52 Z. He and F. Mansfeld, *Energy Environ. Sci.*, 2009, **2**, 215.

53 C. Fernandez-Sanchez, C. J. McNeil and K. Rawson, *Trends Anal. Chem.*, 2005, **24**, 37.

54 A. E. Radi, J. L. Acero Sanchez, E. Baldrich and C. K. O'Sullivan, *J. Am. Chem. Soc.*, 2006, **128**, 117.